Phys. Status Solidi A **210,** No. 5, 1000–1005 (2013) / **DOI** 10.1002/pssa.201200742

Part of Special Section on
Engineering of Functional Interfaces

physica status solidi a
www.pss-a.com
applications and materials science

Synthesis and characterization of Al–Mg–Zn thin film alloys co-deposited from vapour phase

Michael Voith, Andrei I. Mardare, and Achim Walter Hassel*

Institute for Chemical Technology of Inorganic Materials, Johannes Kepler University, Altenberger Str. 69, 4040 Linz, Austria

Received 21 September 2012, revised 23 January 2013, accepted 4 February 2013
Published online 7 March 2013

Keywords aluminium–magnesium–zinc alloys, thin films, co-deposition, downstream analytics

* Corresponding author: e-mail achimwalter.hassel@jku.at, Phone: +43 732 2468 8700, Fax: +43 732 2468 8905
Web: www.jku.at/ictas

Mg–Zn thin film alloys were produced by thermal co-evaporation using single source and dual source geometries. The films containing high amount of Zn (66 at.%) were prone to formation of metallic micro spheres on the surface when high evaporation rates (10 nm s^{-1}) were used. The Mg–27.1 at.% Zn bulk alloy was found to be suitable for co-deposition with Al for producing Al–Mg–Zn thin film alloys. A low Al concentration gradient (5 at.%) could be obtained along the sample due to the high deposition rates of Mg–Zn (7.5 nm s^{-1}) combined with low Al deposition rates (0.2 nm s^{-1}). The Al–Mg–Zn thin films showed an improved resistance against chemical attack when higher amounts of Al are used, as shown by downstream analytics investigations using a flat flow electrochemical cell coupled to an AAS system.

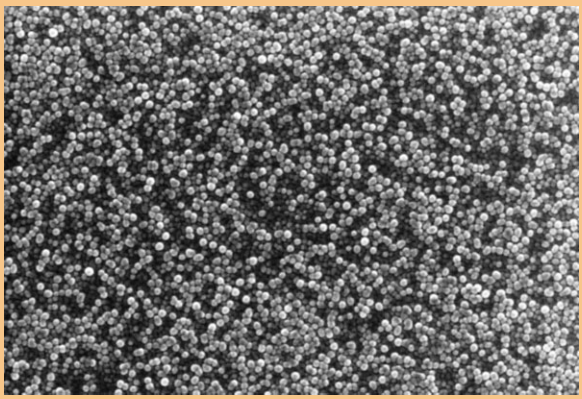

1 Introduction Over the past decades, corrosion protection of steel lead to the development of various metallic coatings [1]. In order to understand the corrosion mechanism in these complex multiphase systems it is necessary to use different analytical and electrochemical techniques or even combinations thereof [2–5]. One of the most prone materials to chemical attack in corrosion protection of steels is Zn. For minimizing its dissolution rate, a lot of effort is put into the tuning of metallic alloy coatings to enhance the corrosion protection [6]. One of the most widely used alloying elements with Zn is Mg, due to the formation of stable intermetallic phases which show higher corrosion resistance [7–11]. Apart from this, Mg is a non-toxic and relatively cheap material, easily implemented into industrial hot dip galvanizing processes. Another material presenting a high potential in corrosion protection is Al that is used for other coating alloys such as Galvalume. Alloying of Mg–Zn with Al can dramatically improve the corrosion resistance in bulk materials [12, 13]. This happens already for low amounts of Al. Unfortunately, the study of bulk metallic alloys is always hindered by the sample fabrication itself which allows only the production of a single alloy at a time.

In the present work, a method for preparation of multielement combinatorial thin films using thermal co-evaporation from different sources is presented. Thin film alloys with a compositional gradient of the alloying elements are obtained on single substrates. Local investigation of various areas on the surface may lead towards high throughput analysis and/or properties screening. The possibility of the production of material libraries opens the door to selectively investigate the chemical behaviour of alloys with well known compositions.

2 Experiments

2.1 Source materials For the production of high quality Al–Mg–Zn thin films with a certain composition it is necessary to use proper source materials for thermal

evaporation. In this work, a bulk alloy composed of Mg−27.1 at.% Zn (provided by voestalpine Stahl GmbH) was used directly as source material for thin film formation and as pre-alloy for the production of $MgZn_2$. At a later stage, $MgZn_2$ was also used as a bulk source for thin film formation. For the production of bulk $MgZn_2$ the Mg−27.1 at.% Zn was enriched with pure Zn (Roth, Karlsruhe, Germany). The alloying of the components was performed in an induction furnace with a maximum power of 10 kW (Linn – High – Therm GmbH, Eschenfelden, Germany). To avoid oxidation of the molten materials the melting and casting procedure was done in a pivotable casting chamber. Prior to the heating procedure, the chamber was evacuated down to a pressure of 1 Pa and afterwards purged with Varigon® H6 (Linde). This procedure was repeated for several times to ensure the removal of oxygen and provided a reducing atmosphere for the melting process. Boron nitride spray was used as a separating agent to coat the inner side of the mould ($20 \times 20 \times 200\,mm^3$). This coating avoids sticking of the melt to the inner walls of the mould and enables an easy remove of the ingot after casting.

2.2 Thermal evaporation Thermal evaporation of the different Mg–Zn bulk materials was done using a co-evaporation setup (Fig. 1). The setup consists of a stainless steel vacuum chamber evacuated by a rotary vane pump (roughing pump) together with an oil diffusion pump. This ensures a base pressure of approximately 10^{-4} Pa. Evacuation of the system is necessary to increase the mean free path of atoms in the vapour phase as well as to avoid the oxidation of the resulting thin films. The bottom flange of the vacuum chamber supported by pneumatic pistons is mobile for allowing the exchange of source materials. Thick copper rod feed-throughs with negligible resistance were used for electrically contacting the thermal sources inside the vacuum. The substrates used were borosilicate glass microscope slides ($75 \times 25\,mm^2$). Pieces of the bulk source material were placed into alumina crucibles (2 ml) surrounded by tungsten filaments providing the joule heating necessary for the evaporation process. Throughout the experiment the distance between the evaporation crucibles and the sample surface was held constant to 160 mm. The tungsten filaments were heated by slowly increasing the current provided by power supplies. Computer controlled software ensured a constant heating rate of $1\,W\,s^{-1}$. For both, single and dual source evaporations the deposition rates of the evaporands were continuously measured using quartz microbalances placed directly above the sources. The production of aluminium containing films was done using co-deposition from both sources. The use of a second source for Al is necessary because the vapour pressure of magnesium and especially Zn is much higher than that of Al. Moreover, the Al evaporation requires a temperature that is more than 600 °C higher than that of Zn and Mg at vapour pressure used. This difference would result in a compositional non-uniformity of the films. To avoid this problem, Al was placed in a second crucible which could be heated up independently from the first one until steady state evaporation takes place from both sources. A shutter covering the entire surface of the sample was used for avoiding film formation before a constant flux of the depositing material was achieved. As soon as the thickness of the films reached 300 nm the shutter was closed.

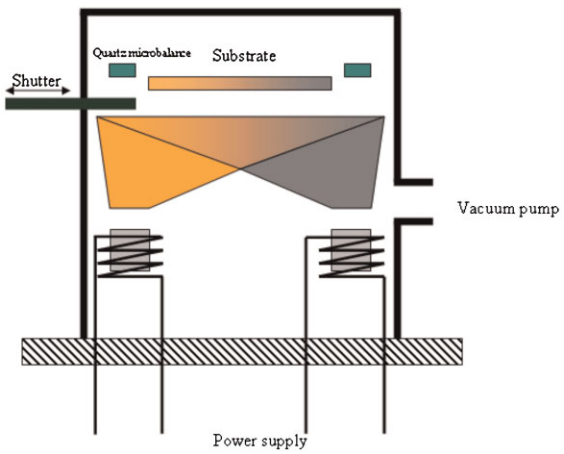

Figure 1 (online colour at: www.pss-a.com) Evaporation setup for co-evaporation of Mg–Zn and Al bulk material sources.

2.3 Analytical methods In this work, a flow cell based method to study dissolution processes of flowing electrolyte in contact with Al−Mg−Zn containing thin films is presented. To perform flow experiments a flat flow cell is directly coupled to an atomic absorption spectrophotometer. This combination allows a continuous quantification of soluble species occurring from dissolution or electrodissolution reactions. In this way, the electrolyte/thin film interfacial reactions can be studied by analysing the outgoing electrolyte. For performing flow experiments, the sample is placed into a flat flow cell (Fig. 2). The cell was machined into an acrylic block containing an inlet and an outlet for the electrolyte flow. A sample holder was tailored from the same material and the sample was fixed between the two blocks using a polymer sealing. The thickness of the sealing determines the volume of the flat flow cell and thus influences the hydrodynamic properties of the system. The sealing also defines the investigated area ($40\,mm^2$) of the film in contact with the passing electrolyte. This geometry allows

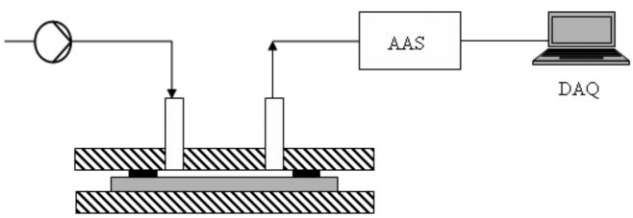

Figure 2 Experimental setup for flow experiments. Arrows indicate the electrolyte flow through the cell.

high exposed area reproducibility and provides a good comparability between different experiments.

Downstream analytics of soluble species in the outgoing electrolyte were carried out by atomic absorption spectroscopy (AAS). A HITACHI Z-8230 Polarized Zeeman Atomic Absorption Spectrophotometer with background correction and a digital data acquisition/processing unit was used. All chemicals used were of analytical grade. A 1000 ppm Zn stock solution was prepared by dissolving proper amounts of ZnO (Merck, Germany) in nitric acid and diluting in deionized water. Standard solutions for calibration were prepared by diluting the standard stock solution. For the quantification of Zn, a hollow cathode lamp with 213.9 nm wavelength and 10.0 mA current was used. The oxidant gas (compressed air) and fuel gas (acetylene) flow rates were 15 and 2.0 L min^{-1}, respectively. Calibration measurements were carried out by measuring blank and standard solutions and the results were fitted by linear regression.

Characterization of the produced bulk materials in terms of composition was done using two different approaches. To check the overall composition of the as-cast ingot, a small piece was cut and solely dissolved in acid. The resulting solution diluted to a volume of 100 ml with deionized water was analysed by atomic absorption spectrometry. For both, bulk materials and thin films, compositional analysis was carried out using energy dispersive X-ray spectroscopy (EDX) and AAS. The microstructural characterization and grain analysis were done using optical microscopy, scanning electron microscopy (ZEISS 1540XB CrossBeam) and atomic force microscopy (Nanosurf Easyscan 2 AFM).

3 Results and discussion

3.1 Source materials Optical microscopy was used for characterizing the surface of the $MgZn_2$ bulk sample as prepared using the induction furnace. The surface was ground and polished in order to obtain a high quality mirror like finish and to allow proper optical imaging as presented in Fig. 3. A uniform grain size distribution with grains of approximately 30 μm can be observed across the sample with clearly visible grain boundaries. The apparent thickness of the grain boundaries varies as a function of location on the sample surface. For most of the grains, the grain boundaries appear to be discontinuous on one side. This is due to the polishing process which partially removed material from and over the grain boundaries which than affected the scattering of light. In order to investigate the differences of composition between the grains and the grain boundaries, high resolution SEM–EDX analysis was performed. These results are summarized in the inlet of Fig. 3. It was found that the grains consist only of $MgZn_2$ and the grain boundaries contain only Zn. This can be explained using the phase diagram of the binary Mg–Zn system [14]. Following the cooling curve from the congruent melting of the intermetallic $MgZn_2$ to temperatures below 600 °C, the eutectic point at approximately 370 °C is reached. At this eutectic temperature a solid solution with a very high content of Zn crystallizes and segregates in the grain boundaries.

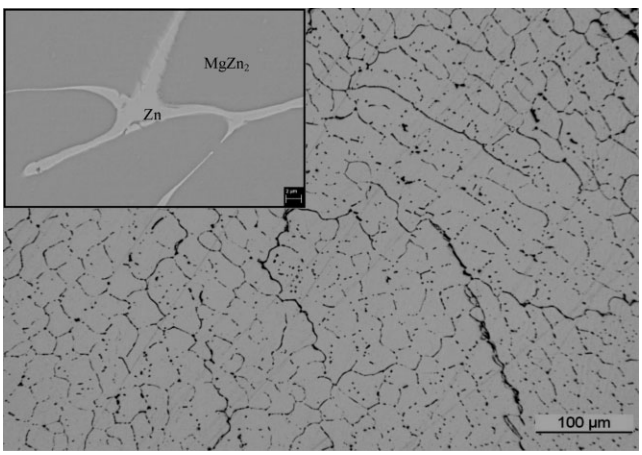

Figure 3 Optical micrograph and SEM image (inset) of a $MgZn_2$ sample.

3.2 Mg–Zn thin films Before the deposition of the ternary Al–Mg–Zn alloy can be performed; detailed studies regarding the deposition of Mg–Zn thin films must be done. This is necessary since the Mg–Zn alloys are deposited from a single source during the co-evaporation with Al. Mg–Zn thin films obtained by thermal evaporation from both bulk materials ($MgZn_2$ and Mg–27.1 at.% Zn) were analysed using SEM–EDX. The quantification of Mg and Zn in the films produced by physical vapour deposition show that the resulting films have exactly the same composition as the bulk source materials used. This can be directly concluded from the results presented in Tables 1 and 2. In both tables, the concentrations of Mg and Zn calculated from the desired chemical composition are presented together with the experimental values. The concentration values calculated in wt.% are also presented due to their wide use in chemistry and metallurgy. Deviations of maximum 1 at.% were found. In principle, this result is somewhat surprising since the thermal evaporation method is known as a non-stoichiometric method. The stoichiometry is usually not conserved due to thermal dissociation of the evaporand. However, in

Table 1 Comparison of calculated and experimentally confirmed composition results for a $MgZn_2$ thin film.

	wt.% Zn	wt.% Mg	at.% Zn	at.% Mg
calculated	84.5	15.5	67	33
experimental	85.1	14.9	68	32

Table 2 Comparison of calculated and experimentally obtained composition results for a Mg−27 at.% Zn thin film.

	wt.% Zn	wt.% Mg	at.% Zn	at.% Mg
calculated	50	50	27.1	72.9
experimental	51	49	27.8	72.2

cases when the evaporation temperatures of individual components are similar or the energy corresponding to the temperature difference is not sufficient for breaking the bonds, there is a higher probability of stoichiometry conservation. This is obviously the case in the present study since the difference in the evaporation temperature of Mg and Zn is only 70 °C. For such cases, it is possible to directly influence the composition of the thin films by the use of carefully chosen source materials.

3.2.1 $MgZn_2$ thin films For analysing the microstructure of the thin films deposited on glass substrates, SEM investigations were performed. In the case of $MgZn_2$ thin films, the heating rate adjustment during the evaporation proofed to be crucial. For high evaporation rates, in the range of 10 nm s^{-1}, the formation of microspheres was observed on the surface of the deposited films. One such sphere is presented in Fig. 4 having a diameter of about 40 μm. These big spheres, as reported to the film thickness, are produced due to high heating rates of the source material resulting in high evaporation rates.

As a result, not only single atoms will be released from the source, but also clusters, or in extension, droplets may be directly set free into the vapour phase. The droplets release from the source is usually known as splashing or spitting and their range is space limited since the heavy droplets start to be affected by gravity. The large distance between the source and the substrate (160 mm) was thought to be sufficient for avoiding the splashed droplets from ever reaching the substrate. However, the SEM results do not provide conclusive information about the origin of the spheres observed on the substrate surface. The possibility that the spheres may grow from the film surface cannot be excluded. In any case, the overall quality of the coating will be affected. This is clearly visible in Fig. 4 were the dominant local feature presented is such a sphere, no other information about the film microstructure being neither visible nor relevant at this scale.

For avoiding the formation of microspheres, the evaporation rate was decreased by at least ten times to values under 1 nm s^{-1}. As a result the sphere formation into the vapor phase was hindered and the surface of the resulting thin films showed no indication of their presence. An SEM image of a $MgZn_2$ thin film deposited with a low deposition rate (<1 nm s^{-1}) is presented in Fig. 5. A fine grain structure can be observed, with grain sizes ranging from 50 to 200 nm.

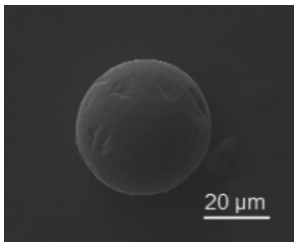

Figure 4 SEM image of a micro sphere on the sample surface.

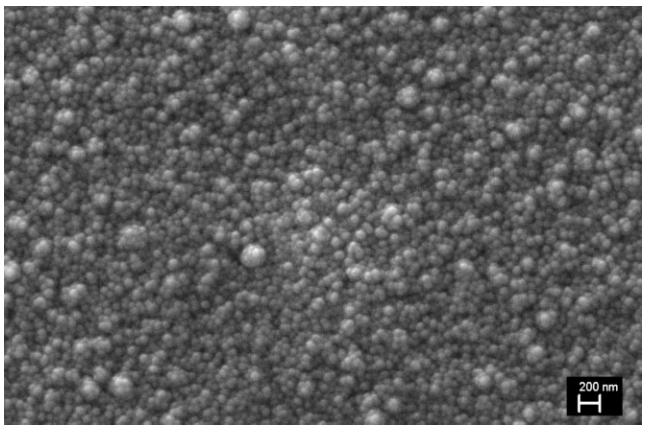

Figure 5 SEM micrograph of a thermally evaporated $MgZn_2$ sample.

The image suggests a low roughness in the nanometer range, with no defects, domains or any type of surface segregation visible. The finer grains form a compact dense packed nanostructure on which the bigger grains lay on. Overall, the quality of the $MgZn_2$ thin films was high enough to allow performing dissolution experiments in which the surface quality plays a major role.

3.2.2 Mg–27.1 at.% Zn thin films The evaporation of Mg−27.1 at.% Zn thin films was performed under conditions identical with the ones used for $MgZn_2$ thin films. Microstructural SEM investigations of films deposited with a low deposition rate (<1 nm s^{-1}) showed that the films are built of highly dense packed small grains with a maximum diameter of 100 nm. This can be observed in the image from Fig. 6. Similar to the previously presented case of $MgZn_2$ thin films, the microstructure shows the same trend. A compact layer formed from smaller diameter grains can be identified under a top layer formed from bigger spherical grains. The Mg−27.1 at.% Zn thin films show a very smooth surface without defects or irregularities. This microstructure

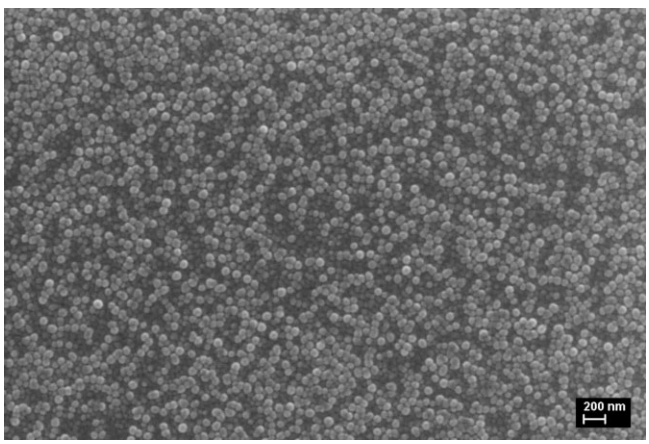

Figure 6 SEM micrograph of a thermally evaporated Mg−27.1 at.% Zn sample.

does not depend on the evaporation rate. Using evaporation rates as high as 10 nm s^{-1} did not result in formation of microspheres on the surface of the films as it happened in the previous case of $MgZn_2$. No relevant microstructural changes could be identified when the evaporation rate of Mg−27.1 at.% Zn was increased by a factor of ten up to 10 nm s^{-1}. From both studies on Mg–Zn thin film formation it can be concluded that the Zn is responsible for the microsphere formation in the vapour phase. Decreasing the Zn amount from 50 to 27.1 at.% resulted in a hindrance of the microspheres nucleation and as a result the evaporation rate does not influence the film microstructure. Complementarily increasing the amount of Mg in the alloy facilitates the transport of both components from the source to the substrate during the formation of Mg−27.1 at.% Zn thin films.

3.3 Al–Mg–Zn films Following the study of Mg–Zn single source evaporation, Al–Mg–Zn thin films were deposited using a second independent aluminium source. A low aluminium concentration in Al–Mg–Zn thin films is sufficient for enhancing the corrosion resistance. Before Al atoms can be released into the vapour phase during thermal evaporation, sufficient energy must be provided for cracking the natural oxide layer present on the surface of the bulk Al source. Due to this well known fact, the evaporation temperature is more than 800 °C and as a result the evaporation itself usually has a bursting character with evaporation rates reaching suddenly values way above 10 nm s^{-1}. There are ways of lowering the evaporation rate of Al (down to 0.1 nm s^{-1}) but usually this leads to hillock formation and stress accumulation in the films [15, 16]. In order to obtain a low concentration of Al during the co-evaporation with a Mg–Zn source a low evaporation rate of Al must be combined with a high evaporation rate of Mg–Zn. For this purpose, the Mg−27.1 at.% Zn was chosen due to the proven independence between microstructural properties and evaporation rates (see 3.2.2).

An Al–Mg–Zn thin film compositional spread was obtained by co-evaporation using an Al evaporation rate of 0.2 nm s^{-1} concomitant with a Mg–Zn evaporation rate of 7.5 nm s^{-1}. The composition was measured by EDX analysis and the entire mapping of the obtained Al–Mg–Zn combinatorial library is presented in Fig. 7. The obtained Al gradient ranged from above 5 at.% at the Al-rich side down to values below 1 at.% Al at the Mg–Zn-rich side of the sample. This is due to the geometry of the co-deposition setup (Fig. 1) combined with the *cos*-law for the thickness variation along the substrate during thermal evaporation [17]. Weak gradients were measured also in the concentration of both Mg and Zn along the sample. This may be attributed to a collision mechanism during the co-evaporation process. Most likely, the heavier Zn atoms are scattering the Mg and Al atoms at the Mg–Zn rich side. When this happens, a decrease in the Mg and Al content in the same time with a complementary increase of the Zn amount can be observed. The individual compositional

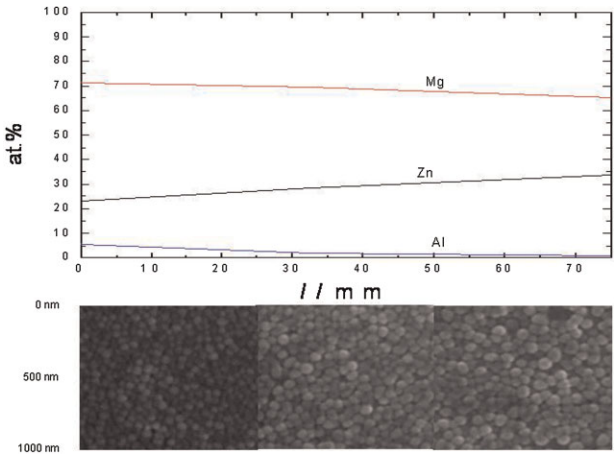

Figure 7 EDX analysis results and SEM images of an Al–Mg–Zn thin film.

gradients can be directly measured from Fig. 7, assuming positive values for an increase from left to right, as −5% for Al, +11% for Zn and −6% for Mg. The overall thin film thickness remains constant along the entire substrate, as confirmed by AFM measurements at various locations along the sample. Differences of maximum 0.5 nm between the measured step profiles were found. The SEM microstructural characterization along the Al−Mg−Zn compositional spread revealed a small gradual change in the grain size of the individual alloys spread along the sample.

In Fig. 7, three different microstructures are presented from left to right corresponding to Al concentrations of 0.7, 1.1, and 5.1 at.%. For the entire compositional spread a compact microstructure can be observed. At high Al concentrations grains of about 50 nm are visible. The grain size increases to approximately 100 nm with the decrease in Al concentration and no hillocks or indications of stress accumulation were found in spite of using low Al deposition rates. Also, no adhesion problems were identified along the entire Al–Mg–Zn compositional spread.

In order to asses the use of Al–Mg–Zn thin film alloys as corrosion protective coatings the chemical attack due to exposure to corrosive media was studied. Investigations of dissolution reactions of the thin films were performed with a flat flow cell setup described before (Fig. 2). The electrolyte used for the experiments was a 0.01 M HCl solution (pH 2.0). Due to the laminar flow inside the cell a uniform exposure of the surface to the electrolyte was ensured. Various areas of the sample were addressed by the flat flow cell for different Al concentrations in the film. The results of the flow experiment with coupled downstream analytics for the determination and quantification of Zn by atomic absorption spectrophotometry in the outgoing electrolyte is shown in Fig. 8 for two different compositions. Because of the defined electrolyte flow rate (3.1 ml min^{-1}), the time dependence of concentration can be directly related to the volume. In Fig. 8 both, time and volume are plotted in the horizontal axis. For all measured concentration over time curves, in the first 10–

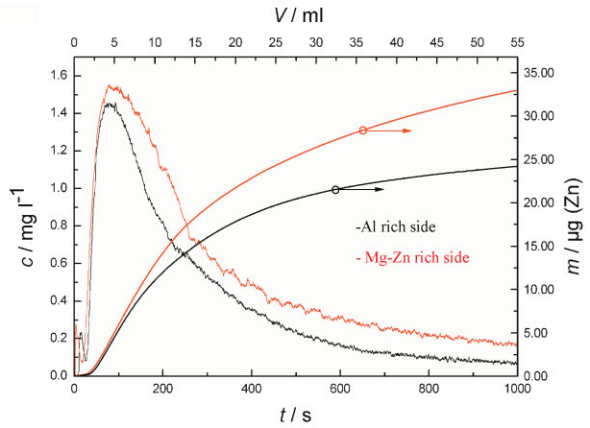

Figure 8 (online colour at: www.pss-a.com) Dissolution curves of an Al–Mg–Zn thin film at different positions on the sample surface.

20 s the cell is filled by pumping the electrolyte through, removing the air and filling the tubing going into the AAS. This results in a time delay described by the small oscillations visible for all curves at the beginning of the experiment. As soon as the air is removed from the closed measurement setup, a laminar steady flow is established and Zn starts dissolving. This is characterized by a rapid increase in the measured Zn concentration in the outgoing electrolyte. From this point on, a decay of the concentration with time can be observed due to the shrinking of the active dissolution area. At the beginning, the entire surface is directly exposed to the flowing corrosive environment but after approximately 100 s the Zn releasing effective area is reduced due to complete local dissolution of the film. This may be named etching through time.

For the same time interval (1000 s), the integration of the area under the curves was performed in order to calculate the total amount of dissolved Zn from the thin film during the experiment. Starting from the compositional gradient of Zn (11 at.%) present along the sample, the ratio between the amount of Zn present at the Mg–Zn rich side and the amount of Zn present at the Al rich side can be calculated as 1.11. However, the ratio of the corresponding Zn amounts dissolved at the two extremes and measured by AAS (after 1000 s) can be directly calculated from Fig. 8 as 1.375. Assuming that on the Mg–Zn rich side there is no (or negligible) corrosion protection, the difference between these ratios must account for a decreased amount of Zn dissolved at the Al rich side. This suggests an improved resistance against chemical attack when higher amounts of Al are used and can be attributed to the self passivation character of Al which is transmitted to a certain extent to the entire alloy thin film.

4 Summary In the present work methods are shown to produce proper bulk material for the synthesis of metallic thin films containing Al, Mg and Zn. Thin films prepared from $MgZn_2$ and Mg−27.1 at.% Zn were characterized by SEM–EDX. It was shown, that the use of Mg−27.1 at.% Zn as a source material results in high quality thin films. To prepare Mg–Zn thin films containing low amounts of Al a dual source thermal evaporator was used. Resulting thin films were analysed by the use of a flat flow cell setup with coupled downstream analytics. Results obtained from the flow experiments obtain information about the composition as well as the chemical behaviour of the thin films in corrosive media.

References

[1] A. R. Marder, Prog. Mater. Sci. **45**, 191–271 (2000).
[2] K. Ogle and S. Weber, J. Electrochem. Soc. **147**, 1770–1780 (2000).
[3] K. Ogle, A. Tomandl, N. Meddahi, and M. Wolpers, Corros. Sci. **46**, 979–995 (2004).
[4] A. Tomandl, M. Wolpers, and K. Ogle, Corros. Sci. **46**, 997–1011 (2004).
[5] C. Commenda, Mater. Charact. **61**, 943–951 (2010).
[6] R. Autengruber, G. Luckeneder, and A. W. Hassel, Corros. Sci. **63**, 12–19 (2012).
[7] T. Prosek, A. Nazarv, U. Bexell, D. Thierry, and J. Serak, Corros. Sci. **50**, 2216–2231 (2008).
[8] N. C. Hosking, M. A. Ström, P. H. Shipway, and C. D. Rudd, Corros. Sci. **49**, 3669–3695 (2007).
[9] B. Schuhmacher, C. Schwerdt, U. Seyfert, and O. Zimmer, Surf. Coat. Technol. **163**, 703–709 (2003).
[10] P. Volovitch, C. Allely, and K. Ogle, Corros. Sci. **51**, 1251–1262 (2009).
[11] S. O. Klemm, J. Schauer, B. Schuhmacher, and A. W. Hassel, Electrochim. Acta **56**, 9627–9636 (2011).
[12] S. Schuerz, M. Fleischanderl, G. H. Luckeneder, K. Preis, T. Haunschmied, G. Mori, and A. C. Kneissl, Corros. Sci. **51**, 2355–2363 (2009).
[13] J. Sullivan, S. Mehraban, and J. Elvins, Corros. Sci. **53**, 2208–2215 (2011).
[14] H. Okamoto, J. Phase Equilib. **15**, 129–130 (1994).
[15] C. Y. Chang and R. W. Vook, J. Vac. Sci. Technol. A **9**, 559–562 (1991).
[16] H. Qiu, F. Wang, P. Wu, L. Pan, L. Li, L. Xiong, and Y. Tian, Thin Solid Films **414**, 150–153 (2002).
[17] S. O. Klemm, A. G. Martin, J. Lengsfeld, J. Schauer, B. Schuhmacher, and A. W. Hassel, Phys. Status Solidi A **207**, 801–806 (2010).